

# Monolithic Pixel Sensors in Deep-Submicron SOI Technology

---

**Marco Battaglia<sup>a,b</sup>, Dario Bisello<sup>c</sup>, Devis Contarato<sup>b,\*</sup>, Peter Denes<sup>b</sup>, Piero Giubilato<sup>b,c</sup>, Lindsay Glesener<sup>a</sup>, Serena Mattiazzo<sup>c</sup>, Chinh Qu Vu<sup>b</sup>**

<sup>a</sup>*University of California at Berkeley,  
Berkeley, CA 94720 (USA)*

<sup>b</sup>*Lawrence Berkeley National Laboratory,  
Berkeley, CA 94720 (USA)*

<sup>c</sup>*Istituto Nazionale di Fisica Nucleare, Sezione di Padova,  
Padova, I-35131, Italy*

*E-mail: DContarato@lbl.gov*

**ABSTRACT:** Monolithic pixel sensors for charged particle detection and imaging applications have been designed and fabricated using commercially available, deep-submicron Silicon-On-Insulator (SOI) processes, which insulate a thin layer of integrated full CMOS electronics from a high-resistivity substrate by means of a buried oxide. The substrate is contacted from the electronics layer through vias etched in the buried oxide, allowing pixel implanting and reverse biasing. This paper summarizes the performances achieved with a first prototype manufactured in the OKI 0.15  $\mu\text{m}$  FD-SOI process, featuring analog and digital pixels on a 10  $\mu\text{m}$  pitch. The design and preliminary results on the analog section of a second prototype manufactured in the OKI 0.20  $\mu\text{m}$  FD-SOI process are briefly discussed.

**KEYWORDS:** Silicon-On-Insulator; Monolithic Pixel Sensors; Particle Detection.

---

\*Corresponding author.

---

## Contents

<b>1. Introduction</b>	<b>1</b>
<b>2. Prototype in 0.15 <math>\mu\text{m}</math> Process</b>	<b>2</b>
2.1 Chip Design and Experimental Setup	2
2.2 Analog Pixels	2
2.3 Digital Pixels	4
2.4 Radiation Hardness Tests	5
<b>3. Prototype in 0.20 <math>\mu\text{m}</math> Process</b>	<b>6</b>
3.1 Chip Design and Experimental Setup	6
3.2 Preliminary Test Results of Analog Pixels	7
<b>4. Conclusions and Outlook</b>	<b>7</b>

---

## 1. Introduction

Silicon on insulator (SOI) technology allows the integration of CMOS electronics on a thin silicon layer which is electrically insulated from the wafer substrate by means of a buried-oxide (BOX). With respect to bulk CMOS processes, the small active volume ensures latch-up immunity and the low junction capacitance enables low-threshold and low-noise operation, thus favoring high-speed and low power digital designs.

SOI Monolithic active pixel sensors for charged particle detection and imaging applications may be built by providing a technology to contact a high-resistivity substrate through the BOX, thus allowing the formation of pixel and biasing implants. With respect to conventional CMOS pixel sensors fabricated on undepleted epitaxial layers, a full CMOS circuitry can be integrated in each pixel and the substrate can be reverse biased and thus depleted for improved charge collection efficiency. A proof of principle of the concept was demonstrated by the SUCIMA Collaboration using a non-commercial, 3  $\mu\text{m}$  feature size process from IET, Poland [1, 2, 3]. Commercial deep-submicron, fully-depleted (FD) SOI CMOS processes were recently made available by OKI, Japan [4] through a collaboration with KEK, allowing for the integration of complex architectures in devices with small pixel pitch. The CMOS electronics is implanted on a 40 nm thin Si layer, which is fully depleted at typical operational voltages, on top of a 200 nm thick BOX contacting a 700  $\Omega\text{-cm}$  Si substrate. A 0.15  $\mu\text{m}$  process was first validated for the fabrication of SOI pixel sensors by KEK in 2006 [5]. Two prototype pixel sensors, featuring both analog and digital pixels have been subsequently designed at LBNL and fabricated in OKI processes. The experimental test results and the performances achieved with the LDRD-SOI-1 chip [6], fabricated in 2007 in the 0.15  $\mu\text{m}$  process, will be summarized in Section 2. Tests of the analog and digital pixels include

in-lab studies of charge collection with infrared lasers and high-energy particle beam tests on a 1.35 GeV electron beam at the LBNL Advanced Light Source. The effects of ionising and non-ionising radiation doses on the chip operation have also been studied. The LDRD-SOI-2 chip was then fabricated in 2008 using a 0.20  $\mu\text{m}$  process, featuring a larger pixel array and a more complex architecture, optimized for faster readout. The chip design and first results obtained on the analog pixels will be presented in Section 3.

## 2. Prototype in 0.15 $\mu\text{m}$ Process

### 2.1 Chip Design and Experimental Setup

The LDRD-SOI-1 chip features an array of  $160 \times 150$  pixels on a 10  $\mu\text{m}$  pitch, subdivided into two analog sections, with thin oxide 1.0 V transistors and thick oxide 1.8 V transistors, and one digital section with 1.8 V bias. The analog pixels implement a simple 3-transistor (3T) architecture, while each digital pixel implement a latch triggered by a clocked comparator, driven by a dedicated readout clock and referenced to an adjustable voltage threshold which is common to the whole matrix. In order to avoid static power dissipation, no amplifier is present in the digital pixels. Like CMOS logic, the comparator consumes power only on clock transitions.

The reverse bias of the sensor substrate increases the potential at the silicon surface, and causes a back-gating effect as the buried oxide may act as a second gate for the CMOS electronics on top, typically causing a shift in the transistor thresholds with increasing depletion voltage. The test of single  $p$ -type and  $n$ -type MOSFETs integrated at the chip periphery showed a threshold shift of  $\sim 200$  mV for a substrate bias of 15 V. The effect had been investigated during the design process by means of TCAD simulations, performed with the Synopsys `Taurus Device` package. The electrostatic potential at the interface between the buried oxide and the silicon substrate was simulated as a function of the substrate bias for different pixel layouts, varying the size of the charge collecting diodes and evaluating the effect of different guard-ring configurations. Simulation showed that the inclusion of a floating  $p$ -type guard-ring around each pixel is beneficial in keeping the field low in the area between diode implants, thus limiting possible back-gating effects on the CMOS electronics on top of the buried oxide. A series of floating and grounded guard-rings were also implemented around the pixel matrix and around the peripheral I/O electronics.

The chips sections are read out independently by a custom FPGA-based readout board with 14-bit ADCs, whose digital outputs are connected to a National Instruments digital I/O PCI board installed on a control PC running a LabView-based data acquisition and on-line data processing program. Pixels are read out at 6.25 MHz clock frequency, with an integration time of 1.382 ms for the analog pixels. Correlated Double Sampling (CDS) is obtained from the subtraction of two frames acquired without resetting the pixels in-between. The integration time for the digital pixels is tunable, and their binary output is buffered through the FPGA to the DIO board on the control PC. Data is stored in the `lcio` format [7]. Offline data analysis is based on a set of dedicated processors developed in the `Marlin C++` reconstruction framework [8].

### 2.2 Analog Pixels

Charge collection as a function of substrate bias has been studied on the analog pixels by means of a 1060 nm infrared laser focused to a  $\simeq 20$   $\mu\text{m}$  spot. Figure 1, left shows the pulse height in a  $5 \times 5$

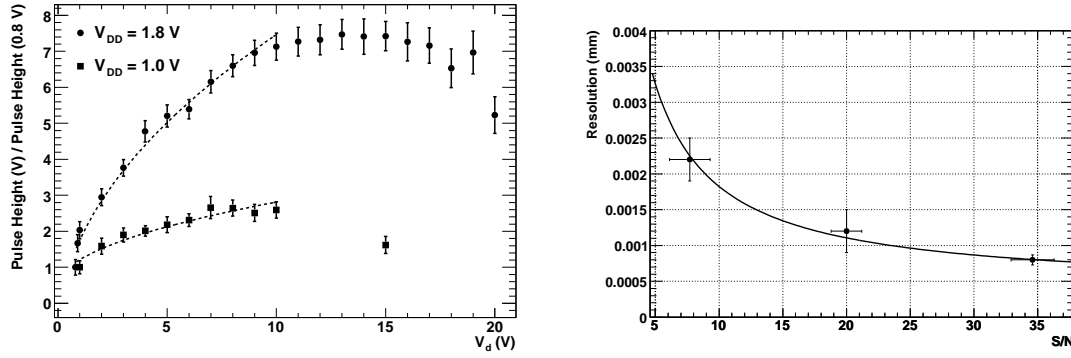


**Figure 1.** Test results of the LDRD-SOI-1 analog pixels with a 1060 nm focused laser. Left: cluster pulse height as a function of the substrate bias,  $V_d$  (from [6]); the data is normalized to the pulse height measured at  $V_d = 0.8$  V. Right: single point resolution as a function of S/N ratio obtained from pixel scans performed with the laser focused to a  $5 \mu\text{m}$  spot, for  $V_d = 7$  V.

pixel matrix centered around the spot center as a function of the applied depletion voltage,  $V_d$ . The signal increases proportionally to the depletion region thickness (equivalently, proportionally to  $\sqrt{V_d}$ ) for  $V_d < 10$  V, while for larger values the signal first saturates and then decreases for  $V_d \geq 15$  V. This is interpreted as due to a back-gating effect, which seems to affect the 1.0 V transistor pixels at lower  $V_d$  values compared to the 1.8 V pixels.

Pixel scans have been performed by focusing a laser beam to a  $\simeq 5 \mu\text{m}$  Gaussian spot and by shifting it in steps of  $1 \mu\text{m}$  along the pixel rows using a stepping motor with a positioning accuracy of  $0.1 \mu\text{m}$ . The pixel spatial resolution could thus be estimated from the spread of the cluster position reconstructed by means of a center of gravity algorithm at each point in the scan. The measurements were repeated for different signal-to-noise ratio (S/N) values, obtained by varying the laser intensity. Figure 1, right shows the results obtained for  $V_d = 7$  V, where data points and error bars represent respectively the mean and r.m.s. of the distribution of the differences between the laser spot position and the reconstructed cluster position. As expected, the measured resolution scales as the inverse of the S/N, and a single point resolution of  $1 \mu\text{m}$  is obtained for S/N ratios of 20 or larger.

The response of the analog pixels to high-momentum charged particles has been tested on the 1.35 GeV electron beam extracted from the booster of the LBNL Advanced Light Source (ALS). Results obtained with the analog pixels have been reported in detail in [6] and are here briefly summarized. Figure 2 shows the cluster pulse height distribution obtained on the 1.8 V pixels for a depletion voltage  $V_d = 10$  V. The distribution is well fitted by a Landau function. Consistently with the measurements performed with infrared lasers, the cluster pulse height was found to increase up to  $V_d = 10$  V, while at 15 V the cluster signal and the efficiency of the chip decreased. The pixel multiplicity in a cluster was found to slightly decrease with increasing  $V_d$ , as expected from an increased electric field in the detector substrate. A S/N ratio of up to 15 was measured with the 1.8 V analog section for  $5 \text{ V} \leq V_d \leq 15 \text{ V}$ .

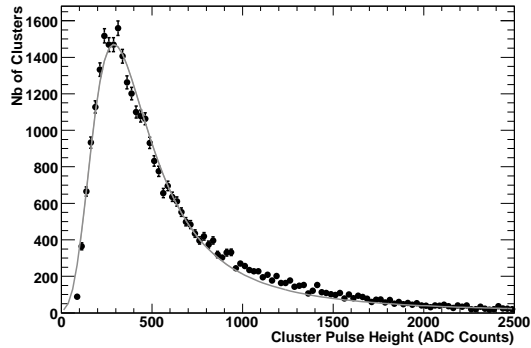


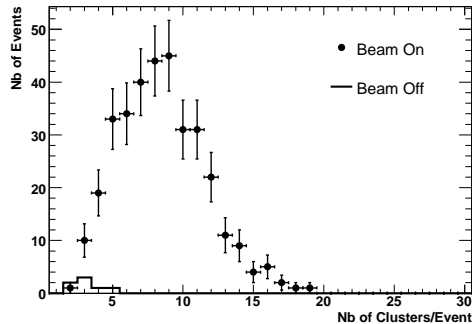
**Figure 2.** Cluster pulse height distribution in the LDRD-SOI-1 1.8 V analog pixels obtained on the 1.35 GeV electron beam at the LBNL Advanced Light Source for a substrate bias  $V_d = 10$  V (from [6]).

### 2.3 Digital Pixels

The ALS 1.35 GeV electron beam was also used to test the response of the LDRD-SOI-1 digital pixels. The pixels are triggered directly by the 1 Hz beam extraction signal and are latched and read out after an integration time of  $10 \mu\text{s}$ . One event is thus acquired per beam spill. For each data set, the first 100 events are used in order to flag noisy pixels, recognized as those which are active in more than 25 events. Furthermore, control data sets have been acquired without beam in order to account for possible background due to noisy pixels which survive the masking and the cluster reconstruction cuts applied in the off-line data analysis.

Beam signals could be observed on the digital pixels only by applying a substrate bias  $V_d \geq 20$  V, and up to  $V_d = 35$  V. As seen in the previous Section, the analog pixels do not function properly above  $V_d \simeq 15$  V. The circuitry in the digital pixels is indeed active only when clocked and is therefore less sensitive to back-gating. Furthermore, back-gating possibly affects the analog threshold of the in-pixel comparators, so that larger substrate voltages are required in order to obtain signals large enough to be above threshold. Figure 3, left shows the hit multiplicity distribution observed with and without beam for  $V_d = 30$  V; an excess of hits in the presence of beam is clearly visible.

Due to the non-uniformity of the beam intensity across the various runs, dedicated data runs have been taken with a single reference detector plane located 2 cm upstream from the LDRD-SOI-1 sensor. The reference plane used was a  $50 \mu\text{m}$ -thin MIMOSA-5 CMOS pixel sensor, developed by IPHC, Strasbourg [9]. The MIMOSA-5 chip features a  $1.7 \times 1.7 \text{ cm}^2$  active area with  $512 \times 512$  pixels on a  $17 \mu\text{m}$  pitch. The performance previously obtained on thin MIMOSA-5 sensors is presented in detail in [10] and [11]. For each run, the number of electron hits reconstructed on the reference plane allowed the particle flux to be monitored in the digital pixel sector active area; the average number of hits per beam spill on the latter was then corrected for the relative change of the beam intensity as determined by the reference plane. Results obtained for different  $V_d$  values are summarized in the Table in Fig. 3, right. From the particle flux reconstructed in the reference layer and its efficiency, as obtained from simulation [11], the efficiency of the LDRD-SOI-1 digital pixels can be estimated to be of the order of 0.3 to 0.5 for  $20 \text{ V} \leq V_d \leq 35 \text{ V}$ . Consistently with what observed for the analog pixels, the average cluster multiplicity was found to decrease as a function of increasing  $V_d$ , i.e. of the increasing electric field in the detector substrate.



$V_d$ (V)	$\frac{Nb.Clusters}{Event}$ beam on	$\frac{Nb.Clusters}{Event}$ beam off	$\langle Nb\ Pixels \rangle$ in Cluster
20	$3.7 \pm 0.1$	0.02	1.78
25	$5.3 \pm 0.1$	0.03	1.32
30	$4.7 \pm 0.1$	0.03	1.26
35	$4.2 \pm 0.1$	0.02	1.14

**Figure 3.** Beam test results of the LDRD-SOI-1 digital pixels. Left: hit multiplicity distribution for 1.35 GeV electrons for a depletion voltage  $V_d = 30$  V and high beam intensity; the continuous line shows for comparison the distribution of fake hits reconstructed in the absence of beam. Right: average number of clusters per event recorded on the LDRD-SOI-1 digital pixels for different values of  $V_d$ , as obtained from the tests performed with a reference plane in front of the detector. Data is reported for beam on (corrected for changes in beam intensity as described in the text) and beam off conditions. The average multiplicity in a cluster is also reported for each  $V_d$  value.

## 2.4 Radiation Hardness Tests

The effect of ionising radiation was preliminarily assessed on single test transistors, irradiated with 30 MeV protons at the BASE Facility of the LBNL 88-inch Cyclotron [12]. The irradiation was performed in steps up to a total fluence of  $2.5 \times 10^{12}$  p/cm<sup>2</sup>, corresponding to a total dose of  $\sim 600$  kRad. The characteristics of two test transistors, one *p*-MOSFET and one *n*-MOSFET, were measured in-between irradiation steps. Both for the *n*-MOS and *p*-MOS transistor, a significant shift in threshold voltage was observed as a function of the increasing dose, the effect being larger for larger substrate biases. For the initial bias of  $V_d = 5$  V the shift was of  $\sim 100$  mV after a fluence of about  $1 \times 10^{12}$  p/cm<sup>2</sup>; a similar shift was measured after the highest fluence for a reduced substrate bias of  $V_d = 1$  V. The total threshold shift is much larger than the one expected at such doses from radiation damage in the transistor thin gate oxide, and seems to be associated with the build-up of positive charge in the detector thick buried oxide, which increases the back-gate potential on the MOS transistors.

The effect of non-ionising radiation has been evaluated on the analog pixel matrix by exposing the sensor to neutrons produced from 20 MeV deuteron breakup on a thin Be target at the LBNL 88-inch Cyclotron [13]. Deuteron breakup produces neutrons on a continuum spectrum from  $\sim 1$  MeV up to  $\sim 14$  MeV. The total neutron fluence was estimated to be  $1.2 \times 10^{13}$  n/cm<sup>2</sup> by means of activation foils placed behind the sensor. The sensor noise has been measured before and after the irradiation as a function of the depletion voltage,  $V_d$ . All tests have been performed at room temperature. A noise increase was observed after irradiation, varying from +25% for  $V_d = 5$  V, to +52% for  $V_d = 20$  V. This is interpreted as due to radiation-induced increase of leakage current in the sensor substrate. The noise of the irradiated chip was subsequently measured as a function of the operational temperature between  $-5^\circ\text{C}$  and  $+20^\circ\text{C}$ , for  $V_d = 10$  V. The noise was observed to decrease with decreasing temperature, consistently with what expected from a leakage current dependence, and the pre-irradiation noise level could be recovered at temperatures below

+5°C.

### 3. Prototype in 0.20 $\mu\text{m}$ Process

#### 3.1 Chip Design and Experimental Setup

A second prototype sensor, the LDRD-SOI-2 chip, has been designed and fabricated in 2008 in the OKI 0.20  $\mu\text{m}$  FD-SOI process, optimized for low leakage current. The chip is a larger scale prototype of  $5 \times 5 \text{ mm}^2$  with an active area of  $3.5 \times 3.5 \text{ mm}^2$  in which  $168 \times 172$  pixels of 20  $\mu\text{m}$  pitch are arrayed (Fig. 4). The pixel matrix is subdivided into a  $40 \times 172$  pixel section with a simple, analog 3T architecture, and in a  $128 \times 172$  pixel section with a new pixel architecture providing a binary output. In the latter, two capacitors are integrated in each pixel for in-pixel CDS, and a digital latch is triggered by a clocked comparator with a current threshold, which is common to the whole matrix. The chip design has been optimized in order to allow readout up to a 50 MHz clock frequency, and the binary section is provided with multiple parallel outputs for high frame rate. As in the LDRD-SOI-1 chip, each pixel is surrounded by a floating  $p$ -type guard-ring; two floating guard-rings also separate the peripheral electronics and I/O logic from the pixel matrix and from the pad area.

The chip is read out by a newly developed DAQ system based on a commercially available FPGA board, deploying the Xilinx Virtex-5 device, connected to a custom-designed ADC board featuring five 14-bit, 100 MS/s ADCs. The chip is mounted on a proximity board which is decoupled from the DAQ hardware. The clock patterns from the FPGA are sent to the chip via LVDS lines, ensuring high speed and low noise over long cable distances, while the chip analog output is connected to one ADC input by a standard USB differential cable. The whole system is connected to the USB bus of a PC, and controlled by a C++ based software interfaced with ROOT classes [14]. The data acquired by the DAQ system is sent to the control PC via the USB bus and stored in the ROOT format, and off-line converted into `lcio` in order to be processed through the Marlin framework (see Section 2.1). Details about the DAQ hardware and software can be found in [15].

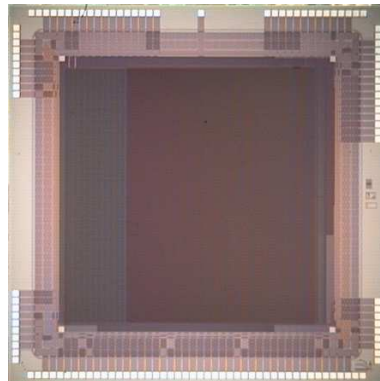


**Figure 4.** Layout of the LDRD-SOI-2 chip, manufactured in the OKI 0.20  $\mu\text{m}$  FD-SOI process.

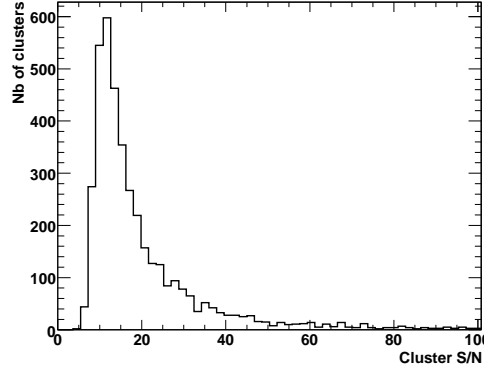


**Figure 5.** Cluster S/N distribution obtained for the analog pixels of the LDRD-SOI-2 chip with 1.5 GeV electrons at the LBNL ALS. The measurement was performed for a clock frequency of 12.5 MHz and a depletion voltage  $V_d = 2$  V.

### 3.2 Preliminary Test Results of Analog Pixels

The LDRD-SOI-2 analog pixels are being tested with a protocol similar to the one used for the LDRD-SOI-1 chip. First tests performed in the lab with infrared lasers show a different behavior of the collected charge signal with the applied substrate bias,  $V_d$ . The signal pulse height increases up to  $V_d = 2$ -3 V and then rapidly saturates. The chip can be properly operated up to  $V_d = 10$  V, however, showing no significant increase in the collected signal. This could be possibly attributed to an increased effect of back-gating due to features of the different fabrication process or to the different guard-ring configuration, and it is currently under investigation.

The analog pixels have been successfully tested with 1.5 GeV electrons at the LBNL ALS up to a pixel clock frequency of 50 MHz, equivalent to an integration time of  $137.6 \mu\text{s}$  for the  $40 \times 172$  pixel array. No significant differences in charge collection have been observed for lower clock frequencies (i.e. longer integration times). A S/N of  $\sim 20$  for reconstructed electron hits is obtained. Figure 5 shows the measured cluster S/N ratio distribution for  $V_d = 2$  V and 12.5 MHz clocking frequency. The pulse height dependence on  $V_d$  is similar to what was observed in the lab with infrared lasers. The chip leakage current and noise performance improves with respect to the  $0.15 \mu\text{m}$  process, and a single pixel noise of  $\sim 30$  ENC has been measured.

## 4. Conclusions and Outlook

Monolithic pixel sensors with analog and digital pixel architectures have been designed and fabricated in SOI technologies that combine deep-submicron CMOS electronics with a high-resistivity substrate in the same device. This is of great interest for many applications, ranging from charged particle detection in high-energy physics to X-ray detection at synchrotron facilities and fast beam imaging, that could benefit from the possibility of integrating complex digital architectures with a depleted silicon substrate yielding larger signals and ensuring a faster charge collection with respect to devices realized in bulk CMOS processes.

A first prototype chip fabricated in a 0.15  $\mu\text{m}$  process has been extensively tested using focused infrared laser beams and a 1.35 GeV electron beam. A S/N ratio of 15 for high energy electrons has been obtained on the analog pixels up to depletion voltages  $V_d = 15$  V, limited by back-gating of the CMOS electronics due to the electrostatic field in the device substrate. A single point resolution of  $\simeq 1$   $\mu\text{m}$  has been estimated from laser scans. The digital pixels appeared to be less affected by back-gating and could be successfully operated at higher substrate biases, up to  $V_d = 35$  V. Preliminary irradiation tests showed an increased effect of back-gating after exposure to ionizing doses, due to positive charge trapping in the buried oxide. A moderate increase of leakage current and consequently of the pixel noise was observed after exposure to  $10^{13}$  n/cm<sup>2</sup>.

A second prototype chip has been fabricated in an optimized 0.20  $\mu\text{m}$  process. The chip implements simple 3T analog pixels and an advanced binary architecture featuring in-pixel charge storage and Correlated Double Sampling, and multiple outputs for high frame rate. First tests of the analog pixels show an improved leakage current performance of this process. A S/N of 20 is found for high-energy electron hits, with single pixel noise figures of 30 electrons, for a readout frequency up to 50 MHz. Further tests of the analog section aimed at understanding the dependence of the collected signal on the depletion voltage are on-going.

## Acknowledgments

This work was supported by the Director, Office of Science, of the U.S. Department of Energy under Contract No. DE-AC02-05CH11231. We thank the staff of the LBNL Advanced Light Source and 88-inch Cyclotron for their assistance and for the excellent performance of the machines. We are also grateful to Prof. Yasuo Arai of KEK for an effective collaboration in the development of SOI pixel sensors.

## References

- [1] J. Marczewski et al., Nucl. Instrum. Meth. A **549** (2005) 112.
- [2] J. Marczewski et al., Nucl. Instrum. Meth. A **560** (2006) 26.
- [3] H. Niemiec et al., Nucl. Instrum. Meth. A **568** (2006) 153.
- [4] OKI Electric Industry Co. Ltd., Japan. <http://www.oki.com>
- [5] T. Tsuboyama et al., Nucl. Instrum. Meth. A **582** (2007) 861.
- [6] M. Battaglia et al., Nucl. Instrum. Meth. A **583** (2007) 526.
- [7] F. Gaede et al., in the *Proc. of 2003 Conf. for Computing in High-Energy and Nuclear Physics (CHEP 03)*, La Jolla, California, 24-28 Mar 2003, pp TUKT001.
- [8] F. Gaede, Nucl. Instrum. Meth. A **559** (2006) 177.
- [9] Yu. Gornushkin et al., Nucl. Instrum. Meth. A **513** (2003) 291.
- [10] M. Battaglia et al., Nucl. Instrum. Meth. A **579** (2007) 675.
- [11] M. Battaglia et al., Nucl. Instrum. Meth. A **593** (2008) 292.
- [12] M.A. McMahan, Nucl. Instrum. Meth. B **241** (2005) 409.

- [13] M.A. McMahan, Nucl. Instrum. Meth. B **261** (2007) 974.
- [14] R. Brun and F. Rademakers, *ROOT - An Object Oriented Data Analysis Framework*,  
<http://root.cern.ch>
- [15] P. Giubilato et al., in the *2007 IEEE Nuclear Science Symposium Conference Record*, October 2008,  
Dresden, Germany.